Received December 5, 2019, accepted December 20, 2019, date of publication December 24, 2019,
date of current version January 6, 2020.

Digital Object Identifier 10.1109/ACCESS.2019.2961935

Predictive Torque Control With Simple Duty-Ratio Regulator of PMSM for Minimizing Torque and Flux Ripples

LETICIA ASEYE ADASE, (Student Member, IEEE),
IBRAHIM MOHD ALSOFYANI, (Member, IEEE),
AND KYO-BEUM LEE, (Senior Member, IEEE)
Department of Electrical and Computer Engineering, Ajou University, Suwon 16499, South Korea

Corresponding author: Kyo-Beum Lee (kyl@ajou.ac.kr)

This work was supported in part by the Korea Electric Power Corporation under Grant R19XO01-20, and in part by the Railroad Technology Research Program funded by the Ministry of Land, Infrastructure and Transport of the Korean Government under Grant 19RTRP-B146008-02.

ABSTRACT In this paper, a new method for reducing the ripples of torque and flux is proposed for the predictive torque control (PTC) of permanent magnet synchronous motors. The conventional PTC uses equations to analyze the relationship between the electrical torque and voltage with a fixed magnitude of reference voltage. Consequently, flux and torque ripples increase significantly at low-speed operation. This paper proposes an improved PTC algorithm using a simple duty-ratio regulator. The proposed method will minimize the torque error by calculating an appropriate torque minimization function to mitigate the induced torque and flux ripple at low speed operation. This torque minimization function is synthesized into the space vector pulse-width modulation block to reduce the torque ripple induced owing to the fixed time duration. The proposed scheme considerably reduces the torque and flux ripples and establishes a fast-dynamic response of the torque in the transient state. Simulation and experimental results show that the proposed method achieves a more efficient steady-state performance and a faster step response compared with the conventional PTC.

INDEX TERMS Flux ripple reduction, permanent magnet synchronous motor, predictive torque control, torque ripple reduction.

NOMENCLATURE

$\boldsymbol{v_s}$	Stator voltage.
$\boldsymbol{\lambda_s}$	Stator flux.
$\boldsymbol{\lambda_r}$	Rotor flux.
$\boldsymbol{i_s}$	Stator current vector.
R_S	Stator resistance.
L_s	Motor inductance.
T_e	Electromagnetic torque.
T_e^*	Reference value of torque.
θ_r	Rotor flux vector position.
θ_s	Stator flux vector position.
θ_{sr}	Angle between θ_r and θ_s position.
D_r	Torque ripple minimization function.
T_s	Digital signal processor (DSP) control cycle.
k_t	Time duration of voltage vector.
v^a	Torque slope active voltage vector.
v^z	Torque slope zero voltage vector.
T_{ripp}	RMS value of the torque ripple.
λ_{ripp}	RMS value of the flux ripple.

The associate editor coordinating the review of this manuscript and approving it for publication was Xiaodong Sun.

I. INTRODUCTION

Permanent magnet synchronous motors (PMSMs) have several advantages over other motors, such as higher power density, high-performance motion control, higher speed, and higher accuracy. Consequently, they are widely used in many automation processes and robotics. Studies have also been conducted on PMSM drives using various torque control methods [1]–[4].

In the last few decades, two control strategies for electrical drives have dominated high-performance industrial applications: field-oriented control (FOC) and direct torque control (DTC) [5], [6]. The DTC of PMSM drives has gained popularity in advanced motor drive applications because it offers a fast-instantaneous motor torque and stator-flux control with simple implementation. The DTC method independently

controls the torque and stator flux and estimates the stator flux using stator voltage and current information. This method compares the calculated and reference torques obtained from the estimated stator flux and determines the voltage vector of the inverter to minimize the error for every control period by comparing it with the hysteresis bandwidth.

The DTC can obtain a fast-dynamic response with a simple control structure [7]. However, as this scheme is based on hysteresis comparators, it suffers from major drawbacks for digital implementation, namely, variable switching frequency, large torque ripple, and high sampling requirements. In addition, its restricted use of the voltage vector is unsuitable for accurate torque control.

Although DTC is preferred over FOC owing to its simplicity and better torque control in steady- and transient-state conditions, some limitations such as high torque ripple [8], variable switching frequency behavior, and problems at low-speed operation still exist. Numerous methods have been proposed to mitigate the shortcomings of these control strategies [9]–[14].

Recent studies have investigated model predictive control (MPC) [15], [16], which is mainly based on the prediction of future system behavior to calculate the optimal execution variables. MPC can be classified into continuous control set MPC (CCS-MPC) [17] and finite control set MPC (FCS-MPC) [18]. In a motor drive system, according to different control objectives, the FCS-MPC method can be classified into model predictive current control [19] and model predictive torque control (MPTC) [20]. This strategy utilizes a control target model to achieve the state variables [21], [22] and uses a correct cost function for each control and conditions defined through reference values and feedback state values to anticipate the output state. Thus, the MPTC strategy uses optimized states as a control input to obtain a minimized cost function for each control period. MPTC considers the stator flux and electromagnetic torque as the control objectives. As it uses one voltage vector at each control period, the ripples of torque and flux increase as in the case of DTC. Thus, in exact control systems, the voltage vectors are divided to mitigate the ripple issue, which results in numerous mathematical calculations [23] and increased computational burden, which have not been solved yet.

Another widely used control strategy is predictive torque control (PTC), which is a subset of CCS-MPC. In contrast to DTC, PTC uses a mathematical approach in the calculation of voltage vectors in the control of PMSM torque while using the relation among torque, flux, and voltage instead of a lookup table. This method has a simple control configuration with fast dynamic torque response. However, similar to DTC, the ripple components in the torque and flux waveforms increase and the harmonic distortion of the PMSM current also increases [24]. The drawback of this method is the fixed time duration of the voltage vector. This results in a limitation of voltage vector choices in the inverter, producing larger torque ripple and higher total distortion in the current.

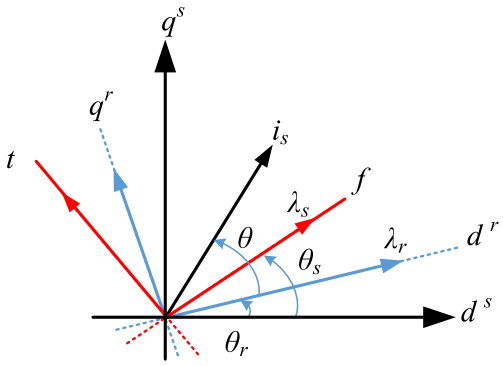

FIGURE 1. Space vector diagram with different coordinate axes of PMSM.

Another work [25] proposed a method to vary the time duration of the voltage vector through mathematical derivations. This method reduced the ripples of torque and flux but added complexity to the system and also degraded the quality of torque and flux in the low-speed region. Thus, there was an increase in torque and flux ripples in the low-speed region.

This paper proposes a simple duty-ratio regulation method for reducing both torque and flux ripples while maintaining the fast-dynamic characteristics of conventional PTC for a three-phase two-level inverter-driven PMSM drive. The proposed method applies an accurate and required voltage for the control of the torque and flux. In this case, the time duration of the voltage vector is not varied but is fixed to achieve a fast-dynamic response, as in the case of the conventional PTC [24]. A simple algorithm that utilizes the information of the stator flux and torque error is later introduced into the space vector pulse-width modulation (SVPWM) block to reduce the torque ripple induced owing to the fixed time duration. The proposed method is validated using PSIM simulation and experiment results.

II. MATHEMATICAL MODEL OF PMSM

Based on the stationary reference frame $d^s - q^s$, a synchronous reference frame $d^r - q^r$ can be obtained using complex vectors as shown in Fig. 1. The synchronized rotating reference frame with stator flux is the $f - t$ reference frame where the rotor flux vector position is θ_r, the stator flux vector position is θ_s. The sum of the resistive voltage drop and the derivative of the flux linkages yields the stator voltage of the PMSM, which is expressed as

$$\boldsymbol{v_s} = R_s \boldsymbol{i_s} + \frac{d\boldsymbol{\lambda_s}}{dt} \tag{1}$$

where $\boldsymbol{v_s} = [v_{dss}, v_{qss}]^t$ is the stator voltage, $\boldsymbol{i_s} = [i_{dss}, i_{qss}]^t$ is the stator current, $\boldsymbol{\lambda_s} = [\lambda_{dss}, \lambda_{qss}]^t$ is the stator linkage flux, and R_s is the stator resistance. The equations of the stator flux in the stationary frame and the electromagnetic torque are expressed, respectively, as

$$\boldsymbol{\lambda_s} = L_s \boldsymbol{i_s} + \boldsymbol{\lambda_r} \tag{2}$$

$$T_e = p\boldsymbol{\lambda_s} \times \boldsymbol{i_s} \tag{3}$$

where L_s is the inductance in the stator, $\boldsymbol{\lambda_r} = [\lambda_r \cos\theta_r, \lambda_r \sin\theta_r]^t$ is the rotor flux, and p is the number of pole pairs.

III. PROPOSED PTC METHOD RESULTS

A. MOTOR TORQUE VERSE VOLTAGE VECTORS

First, the relationship between $\boldsymbol{v_s}$ and T_e is obtained to implement PTC. The rate of change of the motor torque can be obtained using the substitute differential form of (1), (2), and (3) as follows:

$$\frac{d}{dt}T_e = \left(\frac{p}{L_s}\boldsymbol{\lambda_s} \times \boldsymbol{v_s} + p\boldsymbol{v_s} \times \boldsymbol{i_s}\right) - \left(\frac{R_s}{L_s}T_e + \frac{p}{L_s}\boldsymbol{\lambda_s} \times \frac{d\boldsymbol{\lambda_r}}{dt}\right) \tag{4}$$

The motor torque can be controlled by controlling the voltage vector $\boldsymbol{v_s}$ to achieve its desired value if $\boldsymbol{i_s}$, $\boldsymbol{\lambda_s}$, and $\boldsymbol{\lambda_r}$ is known.

From (4), supposing that T_s is the control period and k_t (fixed value $\times$ the control period) is the time duration of the active voltage vector, the voltage vector cycle and the rate of change T_e can be deduced based on the influence of the active voltage vector ΔT_e^a as follows:

$$\Delta T_e^a = \left(\frac{p}{L_s}\boldsymbol{\lambda_s} \times \boldsymbol{v_s} + p\boldsymbol{v_s} \times \boldsymbol{i_s} - \frac{R_s}{L_s}T_e - \frac{p}{L_s}\boldsymbol{\lambda_s} \times \frac{d\boldsymbol{\lambda_r}}{dt}\right) k_t \tag{5}$$

whereas the rest of the cycle ($T_s - k_t$) where the zero-voltage vector influences the rate of change of torque (ΔT_e^z) is expressed as

$$\Delta T_e^z = \left(-\frac{R_s}{L_s}T_e - \frac{p}{L_s}\boldsymbol{\lambda_s} \times \frac{d\boldsymbol{\lambda_r}}{dt}\right)(T_s - k_t) \tag{6}$$

The sum of $\Delta T_e^z + \Delta T_e^a$ is the total increment of the torque in a full control cycle and is expressed as

$$\Delta T_e = \left(\frac{p}{L_s}\boldsymbol{\lambda_s} \times \boldsymbol{v_s} + p\boldsymbol{v_s} \times \boldsymbol{i_s}\right) k_t - \left(\frac{R_s}{L_s}T_e + \frac{p}{L_s}\boldsymbol{\lambda_s} \times \frac{d\boldsymbol{\lambda_r}}{dt}\right) T_s \tag{7}$$

From (7), the relationship between $\boldsymbol{v_s}$ and the change in the torque ΔT_e is established. The motor torque is accurately controlled using the calculated voltage values.

The position angle of the vector θ is proportional to the rotor position angle and can be acquired through a position sensor on the rotor.

As shown in Fig. 1, considering a vector $\boldsymbol{\lambda_r}$ as the position reference, the control voltage can be more accurately oriented. Accordingly, the relationship between $\boldsymbol{v_s}$ and λ_s is determined as follows:

$$\Delta T_e = p\left(\frac{1}{L_s}(\boldsymbol{\lambda_s} - L_s i_s) \times \boldsymbol{v_s}\right) k_t + \left(-\frac{R_s}{L_s}T_e - \frac{p}{L_s}\boldsymbol{\lambda_s} \times \frac{d\boldsymbol{\lambda_r}}{dt}\right) T_s \tag{8}$$

Based on the magnitude of the voltage vector $\boldsymbol{v_s}$, the voltage control angle θ can be derived as

$$\theta = \arcsin\left(\frac{\Delta T_e + \frac{1}{L_s}\left(R_s T_e + p\boldsymbol{\lambda_s} \times \frac{d\boldsymbol{\lambda_r}}{dt}\right) T_s}{\frac{p}{L_s}|\boldsymbol{\lambda_s}|\,|k_t \boldsymbol{v_s}|}\right). \tag{9}$$

The purpose of the angle θ is to decide the proper direction of the reference voltage vector v_s^* for making the torque error ΔT_e zero. This angle θ is the phase difference between the inverter voltage $\boldsymbol{v_s}$ and rotor flux $\boldsymbol{\lambda_r}$. It determines the direction of the voltage vector.

B. STATOR FLUX CONTROL

From Fig. 1, $\boldsymbol{\lambda_s}$ is therefore synchronized to the f–t rotating frame as indicated in Fig. 2. As shown in Fig. 2, the f-axis represents $\boldsymbol{\lambda_s}$, whereas the t-axis represents T_e. The two dotted lines divide the f–t rotating frame into four quadrants (or areas). Each area is characterized by the signs of T_e and $\boldsymbol{\lambda_s}$ as indicated in Table 1. There is either an increase or a decrease in T_e and $\boldsymbol{\lambda_s}$ when the selected $\boldsymbol{v_s}$ is situated inside one of the quadrants. For instance, the selected voltage vector is located in Area II when T_e increases and $\boldsymbol{\lambda_s}$ decreases. Fig. 3 shows the relation among $\boldsymbol{v_s}$, $\boldsymbol{\lambda_r}$, and $\boldsymbol{\lambda_s}$. When T_e increases, $\boldsymbol{\lambda_s}$ leads $\boldsymbol{\lambda_r}$ by an angle θ. In contrast, when T_e decreases, $\boldsymbol{\lambda_s}$ lags behind $\boldsymbol{\lambda_r}$ by an angle θ.

In addition, the magnitude of the stator flux increases if the phase difference between $\boldsymbol{v_s}$ and $\boldsymbol{\lambda_s}$ is within $\pm 90°$ and vice versa. To control $\boldsymbol{\lambda_s}$, the angle of $\boldsymbol{v_s}$ is determined as follows: the magnitude of $\boldsymbol{\lambda_s}$ must increase at $\Delta\theta = \theta$; otherwise, the magnitude of $\boldsymbol{\lambda_s}$ must decrease at $\Delta\theta = \pi - \theta$.

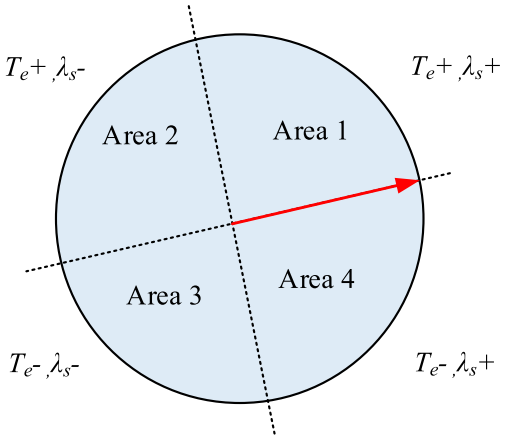

FIGURE 2. Phase plane division for the control of torque and stator flux.

TABLE 1. Areas of voltage vectors.

Regions	Definition
Area 1	Torque increases, Flux increases
Area 2	Torque increases, Flux decreases
Area 3	Torque decreases, Flux decreases
Area 4	Torque decreases, Flux increases

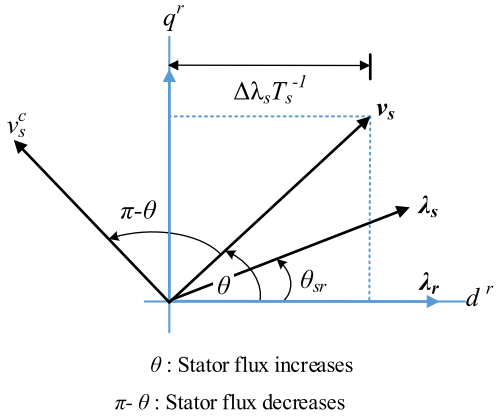

FIGURE 3. Predictive torque control strategy.

A strategy for a further reduction of the torque ripple is described in the following section.

C. TORQUE MINIMIZATION STRATEGY

The fixed value k_t mentioned in [24] induces a torque ripple although $\Delta\lambda_s$ is near zero when controlled because the information of the flux error is not captured in (9). The strategy for torque ripple reduction proposed in this paper involves a two-step design. The first step involves the determination of hysteresis bandwidth using the error of the stator flux to apply the active voltage required to control the stator flux. From (8), the strategy of PTC can accurately control the motor torque. Therefore, if the output voltage vector of the inverter satisfies (9), the torque error can be almost nullified in the control cycle. $\boldsymbol{v_s}$ is set to a fixed magnitude to simplify the control structure in the PTC method. The magnitude is selected based on its effect on the system. When the magnitude is too small, the dynamic response of the system is degraded, which indicates that a fast step response cannot be achieved. In contrast, the larger the magnitude of voltage (k_t), the larger is the torque ripple, which further degrades the system performance. This study uses a tested value of T_s of 0.75 obtained from [24].

The second step involves the use of a simple mathematical equation that includes the information of the flux error to reduce the torque ripple. From (5), applying a non-zero voltage vector and from applying a zero-voltage vector during a cycle will be rewritten, respectively, as

$$\Delta T_e^a = v^a k_t \tag{10}$$

$$\Delta T_e^z = v^z (T_s - k_t) \tag{11}$$

where v^a is a torque slope active vector and v^z is a zero vector and they can be calculated as:

$$v^a = \frac{p}{L_s}\lambda_s \times v_s + p v_s \times i_s - \frac{R_s}{L_s}T_e - \frac{p}{L_s}\lambda_s \times \frac{d\lambda_r}{dt} \tag{12}$$

$$v^z = -\frac{1}{L_s}\left(R_s T_e + p\lambda_s \times \frac{d\lambda_r}{dt}\right) \tag{13}$$

All variables could be taken as invariant for a small period of time. Thus, the slope torque v^a and v^z are constant within a calculated interval. With the above-mentioned assumption, the torque in every control cycle can then be divided into

$$T_e = \begin{cases} T_e s + v^a t & 0 \le t \le k_t \\ T_e s + v^a k_t - v^z k_t + v^z t & k_t \le t \le T_s \end{cases} \tag{14}$$

where $T_e s$ is the value of the torque at the beginning of the control cycle. Using root means square (RMS) value of the torque error which is the torque ripple between the actual torque and the reference torque over a period of T_s. In this case, torque error is defined as

$$\Delta T_e = T_e - T_e^* \tag{15}$$

Generally, to evaluate the signal performance that has a different value than that of its reference, the RMS is commonly used as expressed below [26]:

$$(\Delta T_{eRMS})^2 = \frac{1}{T_s}\int_0^{T_s} (\Delta T_e)^2 dt \tag{16}$$

or it can be expressed as

$$= \frac{1}{T_s}\int_0^{T_s} (T_e - T_e^*)^2 dt \tag{17}$$

Thus, the square of the RMS torque ripple following the above equations will be:

$$(\Delta T_{eRMS})^2 = \frac{1}{T_s}\int_0^{k_t} (T_e s + v^a t - T_e^*)^2 dt + \frac{1}{T_s}\int_{k_t}^{T_s} (T_e s + v^a k_t - v^z k_t + v^z t - T_e^*)^2 dt \tag{18}$$

The optimal time duration, which in this case is expressed as the torque ripple minimization function (D_r), spent on the voltage vector satisfy the following equation [26]:

$$\frac{\partial \left(T_e - T_e^e\right)^2}{\partial k_t} = 0 \tag{19}$$

Solving the above (19), the optimal solution is obtained as expressed below

$$D_r = \frac{2\Delta T - v^z T_s}{2v^a - v^z} \tag{20}$$

The above equation can be further expanded as follows [27]:

$$D_r = \frac{2\Delta T}{2v^a - v^z} - \frac{2v^z T_s}{2v^a - v^z} \tag{21}$$

It can be deduced from (21) that the first term is proportional to the torque error and the second term includes the zero vector that causes a decrease in the stator flux. Thus, it is

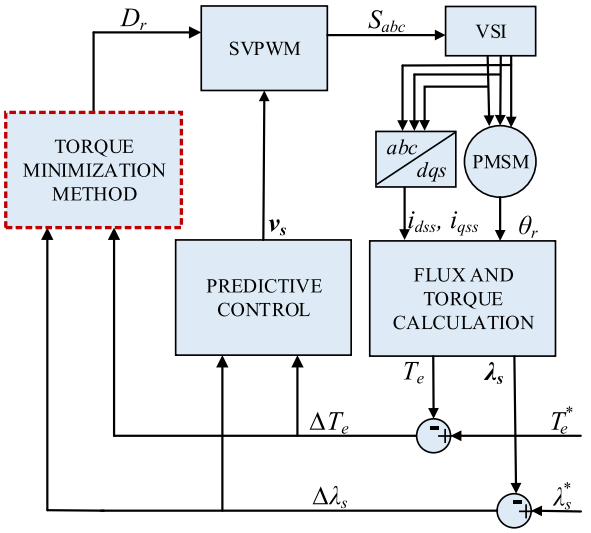

FIGURE 4. Block diagram of PMSM based on the proposed PTC.

TABLE 2. Simulation parameters.

Parameters	Value
Rated power (P_{rated})	11 [kW]
Rated speed (ω_{rated})	1750 [rpm]
Rated torque (T_{rated})	60 [Nm]
Rated current (I_{rated})	19.9 [A]
Stator Resistance (R_s)	0.349 [Ω]
Permanent magnet flux (λ)	0.554 [Wb]
Inductance (L_s)	15.6 [mH]
Inertia (J)	0.021 [kgm^2]
Number of poles (P)	6

concluded that the second term is the flux error [28]. This is rewritten as

$$D_r = T_{ripp} + \lambda_{ripp} \tag{22}$$

where $T_{ripp} = abs(\Delta T_e \,/\, T_{const})$ and $\lambda_{ripp} = abs(\Delta\lambda_s \,/\, \lambda_{const})$. Here, T_{const} is the torque constant, and λ_{const} is the flux constant.

To reduce the torque ripple induced owing to the fixed magnitude of the voltage vector, the study in [25] proposed a method of varying the magnitude of the voltage vector by using the following equation where k_t is the time duration:

$$k_t = \frac{\sqrt{(v_s \sin\theta)^2 + \left(\boldsymbol{\lambda_s} T_s^{-1}\right)^2}}{|v_s|} \tag{23}$$

It can be observed upon applying this concept to the conventional PTC that, although the flux ripple is reduced (because of the introduction of the flux error, which helps drive the flux ripple to zero), the torque ripple is increased further. As this study aims to obtain a fast-dynamic response in the transient state while acquiring minimal torque ripple at the steady state, the following strategy was adopted.

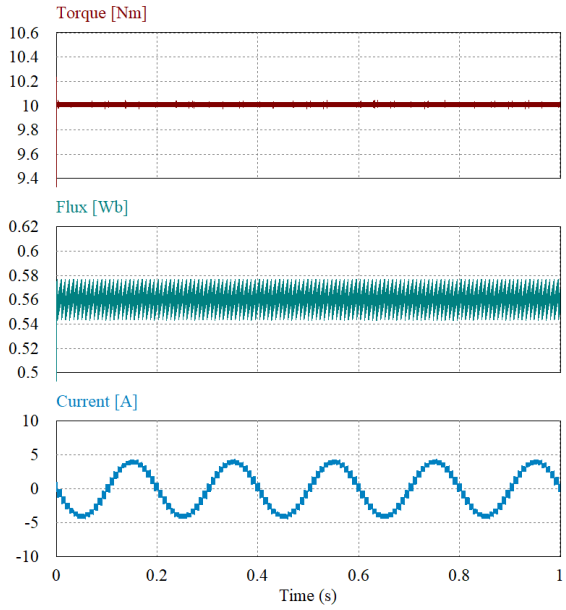

(a)

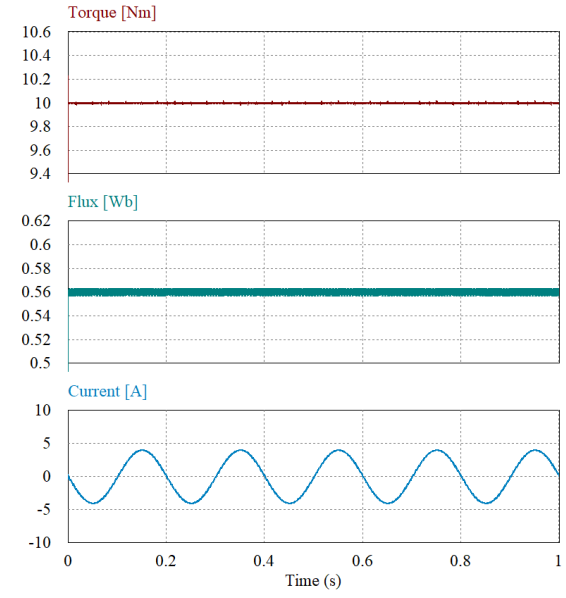

(b)

FIGURE 5. Simulation Results of the motor torque and stator flux at 100rpm. (a) Conventional PTC. (b) Proposed PTC.

Based on the analysis of a degraded/slow dynamic response when the magnitude of the voltage vector is varied, the function derived (D_r) is introduced into the system after the predictive control block as shown in Fig. 4. Thus, the zero vector is applied only at the end of the control period. This reduces the RMS torque ripple significantly. The relationship of the minimization function D_r and the $\boldsymbol{v_s}$ is expressed below

$$\begin{cases} v_{an} = vs_a D_r + v_{offset} \\ v_{bn} = vs_b D_r + v_{offset} \\ v_{cn} = vs_c D_r + v_{offset} \end{cases} \tag{24}$$

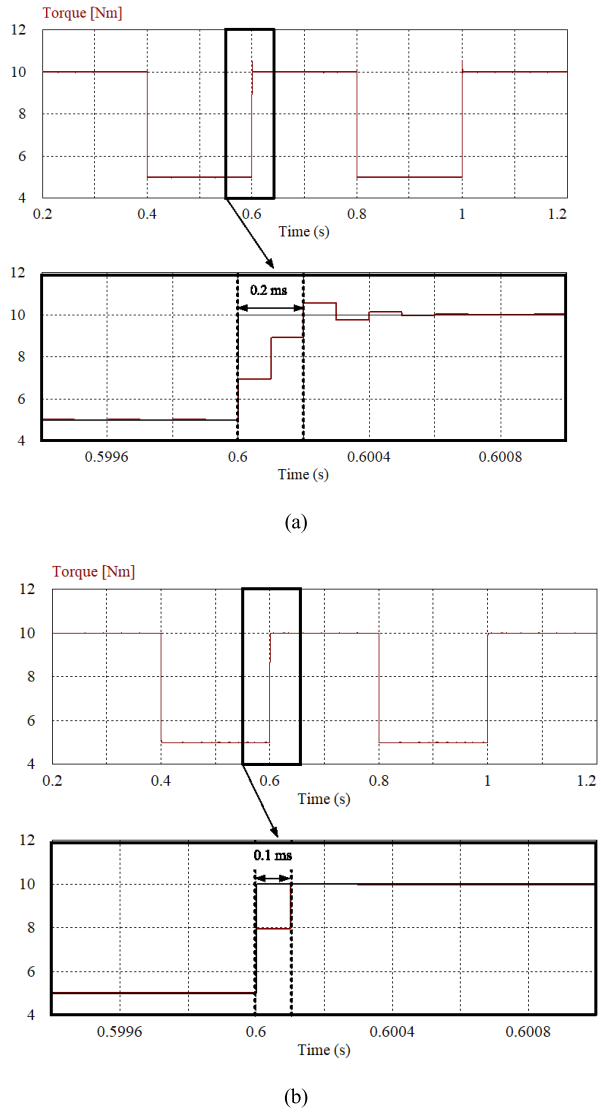

FIGURE 6. Simulation results of the torque step response from 5 to 10 Nm. (a) Conventional TPC. (b) Proposed TPC.

where v_{an}, v_{bn}, v_{cn}, are the reference voltages, where v_{sa}, v_{sb}, and v_{sc} are the phase voltages and v_{offset} is the offset voltage.

The offset voltage is obtained using the maximum (V_{max}) and the minimum (V_{min}) values of the phase voltage references as follows:

$$V_{offset} = \frac{V_{\max} + V_{\min}}{2}. \tag{25}$$

IV. SIMULATION RESULTS

In this section, the effectiveness of the proposed method is compared with that of the conventional method [24] at low speed by using the PSIM software tool. The sampling time of the PTC control scheme was set to 100 μs and the switching frequency of the inverter was set to 10 kHz, in accordance with the experimental setup configuration. The DC-link voltage of 350 V and PMSM power of 11 kW were used in the simulation. The other parameters used are shown in Table 2.

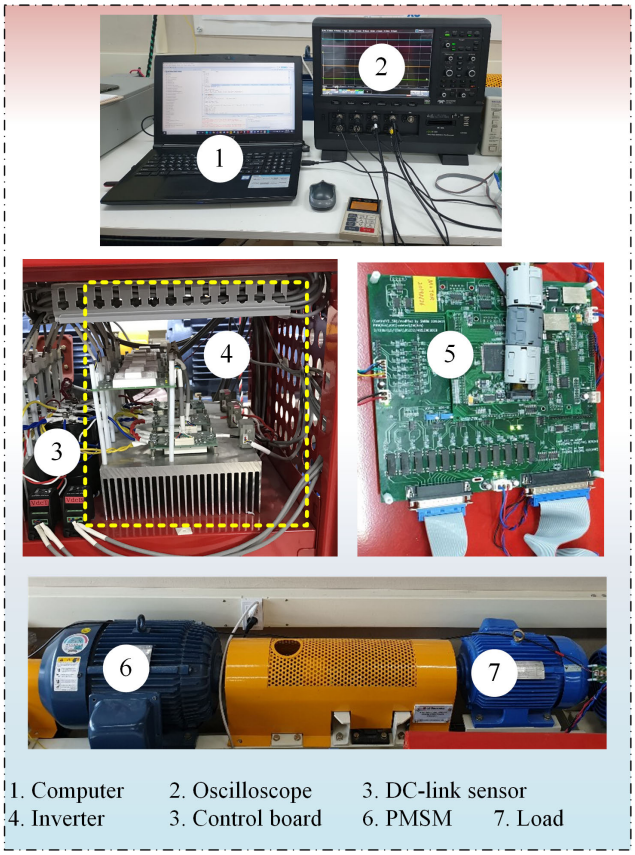

FIGURE 7. Experimental setup.

The RMS values of the torque and flux ripples are calculated based on the following equations [29]:

$$T_{ripp(RMS)} = \sqrt{\frac{1}{N_0}\sum_{k}^{N_0}\left(T_e\,(k) - T_e^{ave}\right)^2} \tag{26}$$

$$\lambda_{ripp(RMS)} = \sqrt{\frac{1}{N_0}\sum_{k}^{N_0}\left(\boldsymbol{\lambda}_s\,(k) - \boldsymbol{\lambda}_s^{ave}\right)^2} \tag{27}$$

where T_e^{ave} is the average values of torque, λ_e^{ave} is the average values of flux and N is a number of samples. For the verification of the proposed method, the conditions for torque minimization include that the rated torque and stator flux values be 10%. Fig. 5 shows the steady-state output torque with a load of 10 Nm and the flux of the two methods at the low speed of 100 rpm, where the ripple of the conventional PTC is 2.5% Nm and that of the proposed method is 1.5% Nm.

Furthermore, the ripple component of the flux decreased from 0.8% Wb for the conventional PTC to almost 0.1% Wb for the proposed method. Fig. 6 shows the dynamic torque response of the conventional and proposed PTC methods. The load was changed from 10 Nm to 5 Nm and vice versa at an interval of 0.2 s. The zoomed result was captured at 0.6 s. It is evident that the proposed method maintains a better response compared with the conventional PTC.

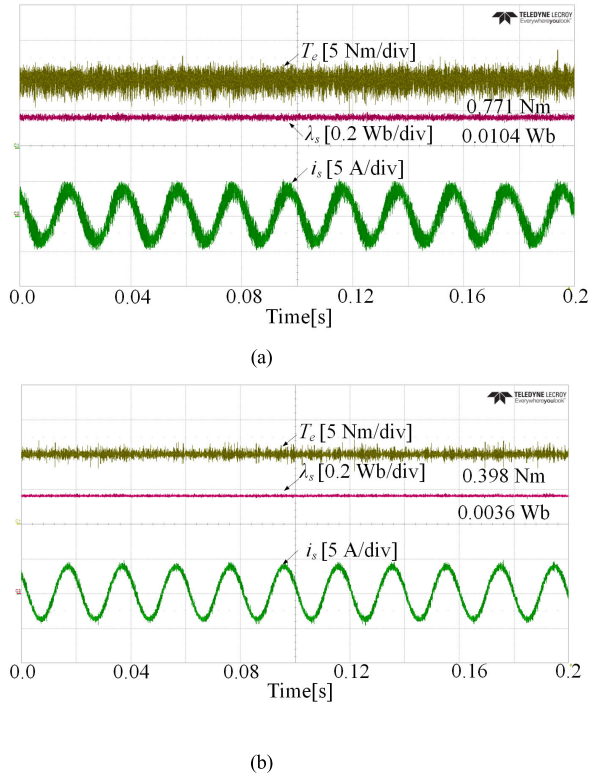

FIGURE 8. Experimental results of the motor torque and stator flux of (a) Conventional PTC. (b) Proposed PTC at 100 rpm.

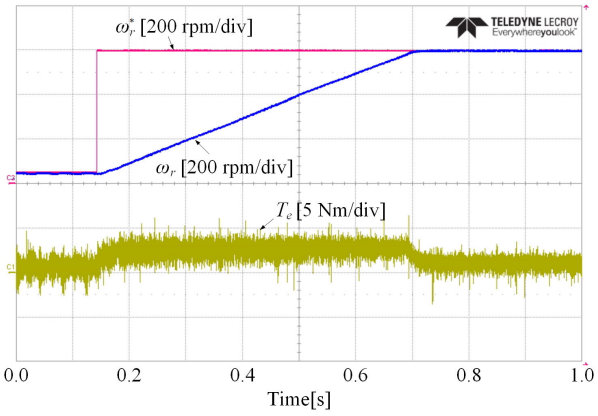

FIGURE 9. Experimental result of the speed step response from 50 rpm to 600 rpm for conventional PTC.

Thus, the proposed method reduced flux and torque ripples compared with those of the conventional method.

V. EXPERIMENTAL RESULTS

The experimental set-up includes a PMSM supplied by a three-phase inverter and driven by the PTC technique, built on a Texas Instruments F28335 DSP with a sampling time of 100 μs. The parameters listed in Table 2 were used. The same sampling period of 100 μs was used to operate the hysteresis controllers, predictive strategy, and SVPWM generation.

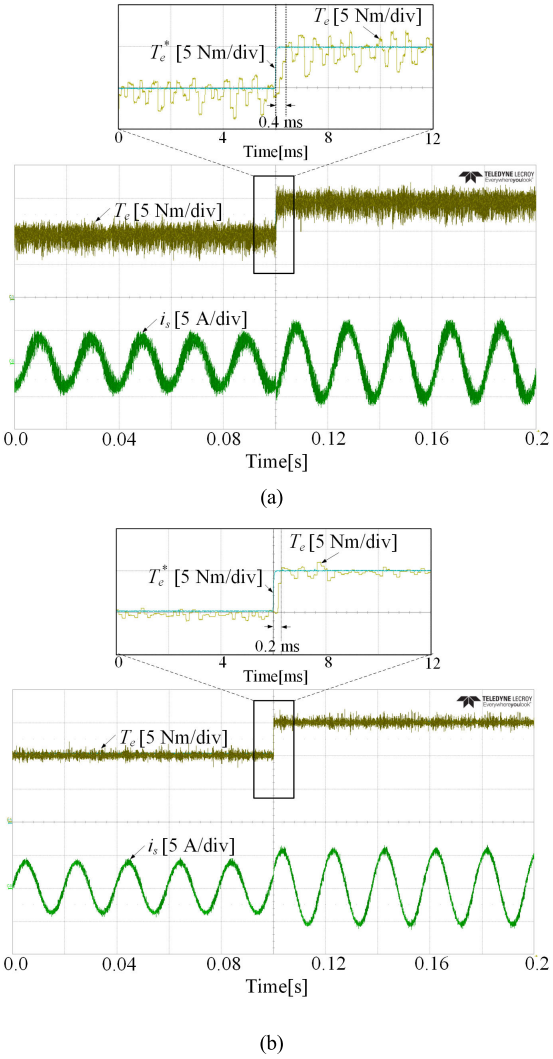

FIGURE 10. Experimental result showing the dynamic torque response of the (a) conventional PTC and (b) proposed PTC at 100 rpm.

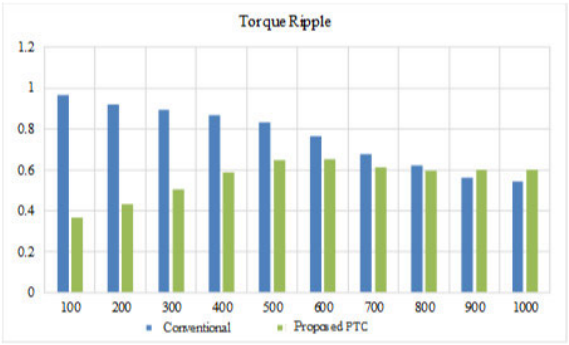

FIGURE 11. Steady-state torque ripple calculation at different speeds.

The switching frequency was set to 10 kHz. The experimental setup is shown in Fig. 7.

The experimental waveforms of the steady-state responses for the conventional and proposed PTC methods are shown in Fig. 8(a) and (b), respectively. A speed of 100 rpm and a

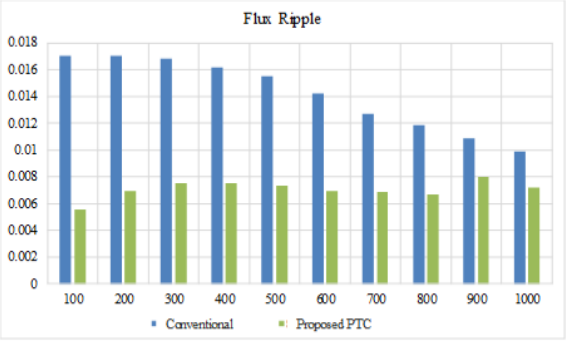

FIGURE 12. Steady-state flux ripple calculation at different speeds.

load of 10.0 Nm are applied to the motor. Ripple calculation for both torque and flux were carried out using (26) and (27) respectively. Fig. 8(a) shows the experimental result of the conventional PTC; as in the simulation, the magnitude of the voltage is fixed at 0.7. Fig. 8(b) shows the experimental result of the proposed PTC method. At the steady state, the torque ripple is decreased from 0.771 Nm in the conventional PTC to 0.398 Nm in the proposed PTC, which is a reduction of approximately 56%. Furthermore, for the conventional method, the stator flux is controlled at the reference flux (λ_s^*) of 0.56 Wb with a flux ripple of approximately 0.01 Wb; however, in the case of the proposed method, the flux ripple is approximately 0.004 Wb with λ_s controlled at 0.56 Wb.

Fig. 9 shows the variable-speed operation at low speed for the conventional PTC method. The motor speed is changed from 50 rpm to 600 rpm with no load. The motor is controlled using the conventional PTC method. In the variable-speed operations, the torque ripple is decreased in the high-speed region, which indicates the drawback of this method in the low-speed region.

Figs. 10(a) and (b) show the dynamic responses of the conventional and proposed PTCs with a load at 100 rpm, respectively, with the zoomed-in torque responses shown above them. It can be observed that the proposed method is efficient in reducing torque ripples, and simultaneously, its dynamic torque response is fast compared to that of the conventional PTC. The dynamic response from 10 Nm to 15 Nm is shown in Fig. 10.

Thus, it is evident that the proposed PTC method improves the performance of a three-phase two-level inverter-fed PMSM drive under all operating conditions. The experimental and quantitative results presented in Figs. 11 and 12 substantiate the superior performance of the proposed PTC over that of the conventional PTC. The experimental results show that the torque and flux dynamics are generally deteriorated as the operating speed is decreased in classical conventional PTC drives, which is reasonable and can be attributed mainly to the speed-dependent nature of the torque variation rate. By contrast, the proposed PTC has been proven to be equally efficient at minimizing torque ripples in the low-speed region.

VI. CONCLUSION

This paper presents a simple and effective method to reduce the ripples of torque and flux for the PTC of PMSMs. The proposed method can accurately control both the flux and torque ripples while improving the dynamic response of the system. The proposed method applies an accurate and required voltage for the control of torque and flux while maintaining a fast step response. In this case, the time duration of the voltage vector is fixed to achieve the fast-dynamic response of the system. A simple duty ratio regulation algorithm containing the information of the stator flux error is introduced into the SVPWM block to reduce the torque ripple induced owing to the fixed time duration. The study focused on low-speed applications considering that the values of the torque and current ripples largely increase for PTC in this region. The simulation results demonstrated that the proposed PTC method effectively improves the system dynamics and greatly reduces the torque ripple compared with those of the conventional PTC method over a wide speed range.

REFERENCES

[1] X. Sun, "MPTC for PMSMs of EVs with multi-motor driven system considering optimal energy allocation," *IEEE Trans. Magn.*, vol. 55, no. 7, Jul. 2019, Art. no. 8104306, doi: 10.1109/TMAG.2019.2904289.

[2] M. Pacas and J. Weber, "Predictive direct torque control for the PM synchronous machine," *IEEE Trans. Ind. Electron.*, vol. 52, no. 5, pp. 1350–1356, Oct. 2005, doi: 10.1109/TIE.2005.855662.

[3] X. Sun, Z. Shi, L. Chen, and Z. Yang, "Internal model control for a bearingless permanent magnet synchronous motor based on inverse system method," *IEEE Trans. Energy Convers.*, vol. 31, no. 4, pp. 1539–1548, Dec. 2016, doi: 10.1109/TEC.2016.2591925.

[4] Z. Zhang and X. Liu, "A duty ratio control strategy to reduce both torque and flux ripples of DTC for permanent magnet synchronous machines," *IEEE Access*, vol. 7, pp. 11820–11828, 2019, doi: 10.1109/ACCESS.2019.2892121.

[5] K.-B. Lee, J.-H. Song, I. Choy, and J.-Y. Yoo, "Torque ripple reduction in DTC of induction motor driven by three-level inverter with low switching frequency," *IEEE Trans. Power Electron.*, vol. 17, no. 2, pp. 255–264, Mar. 2002, doi: 10.1109/63.988836.

[6] I. M. Alsofyani, N. R. N. Idris, and K.-B. Lee, "Dynamic hysteresis torque band for improving the performance of lookup-table-based DTC of induction machines," *IEEE Trans. Power Electron.*, vol. 33, no. 9, pp. 7959–7970, Sep. 2018, doi: 10.1109/TPEL.2017.2773129.

[7] I. Takahashi and T. Noguchi, "A new quick-response and high-efficiency control strategy of an induction motor," *IEEE Trans. Ind. Appl.*, vol. IA-22, no. 5, pp. 820–827, Sep. 1986, doi: 10.1109/TIA.1986.4504799.

[8] A. B. Jidin, N. R. B. N. Idris, A. H. B. M. Yatim, M. E. Elbuluk, and T. Sutikno, "A wide-speed high torque capability utilizing overmodulation strategy in DTC of induction machines with constant switching frequency controller," *IEEE Trans. Power Electron.*, vol. 27, no. 5, pp. 2566–2575, May 2012, doi: 10.1109/TPEL.2011.2168240.

[9] Y. Cho, Y. Bak, and K.-B. Lee, "Torque-ripple reduction and fast torque response strategy for predictive torque control of induction motors," *IEEE Trans. Power Electron.*, vol. 33, no. 3, pp. 2458–2470, Mar. 2018, doi: 10.1109/TPEL.2017.2699187.

[10] I. M. Alsofyani, Y. Bak, and K. Lee, "Fast torque control and minimized sector-flux droop for constant frequency torque controller based DTC of induction machines," *IEEE Trans. Power Electron.*, vol. 34, no. 12, pp. 12141–12153, Dec. 2019, doi: 10.1109/TPEL.2019.2908631.

[11] X. Sun, K. Diao, Z. Yang, G. Lei, Y. Guo, and J. Zhu, "Direct torque control based on a fast modeling method for a segmented-rotor switched reluctance motor in HEV application," *IEEE J. Emerg. Sel. Topics Power Electron.*, to be published, doi: 10.1109/JESTPE.2019.2950085.

[12] A. Xu, C. Shang, J. Chen, J. Zhu, and L. Han, "A new control method based on DTC and MPC to reduce torque ripple in SRM," *IEEE Access*, vol. 7, pp. 68584–68593, 2019, doi: 10.1109/ACCESS.2019.2917317.

[13] X. Sun, J. Cao, G. Lei, Y. Guo, and J. Zhu, "Speed sensorless control for permanent magnet synchronous motors based on finite position set," *IEEE Trans. Ind. Electron.*, to be published, doi: 10.1109/TIE.2019.2947875.
[14] X. Sun, C. Hu, G. Lei, Y. Guo, and J. Zhu, "State feedback control for a PM hub motor based on gray wolf optimization algorithm," *IEEE Trans. Power Electron.*, vol. 35, no. 1, pp. 1136–1146, Jan. 2020, doi: 10.1109/TPEL.2019.2923726.
[15] J. H. Lee, "Model predictive control: Review of the three decades of development," *Int. J. Control Automat. Syst.*, vol. 9, no. 3, pp. 415–424, Jun. 2011, doi: 10.1007/s12555-011-0300-6.
[16] J. Zhao, X. Quan, M. Jing, M. Lin, and N. Li, "Design, analysis and model predictive control of an axial field switched-flux permanent magnet machine for electric vehicle/hybrid electric vehicle applications," *Energies*, vol. 11, no. 7, pp. 1–22, Jul. 2018, doi: 10.3390/en11071859.
[17] I. M. Alsofyani and K.-B. Lee, "Improved deadbeat FC-MPC based on the discrete space vector modulation method with efficient computation for a grid-connected three-level inverter system," *Energies*, vol. 12, no. 16, p. 3111, Apr. 2019, doi: 10.3390/en12163111.
[18] H. T. Nguyen and J.-W. Jung, "Finite control set model predictive control to guarantee stability and robustness for surface-mounted PM synchronous motors," *IEEE Trans. Ind. Electron.*, vol. 65, no. 11, pp. 8510–8519, Nov. 2018, doi: 10.1109/TIE.2018.2814006.
[19] J. J. Aciego, I. G. Prieto, and M. J. Duran, "Model predictive control of six-phase induction motor drives using two virtual voltage vectors," *IEEE J. Emerg. Sel. Topics Power Electron.*, vol. 7, no. 1, pp. 321–330, Mar. 2019, doi: 10.1109/JESTPE.2018.2883359.
[20] T. Geyer, G. Papafotiou, and M. Morari, "Model predictive direct torque control—Part I: Concept, algorithm, and analysis," *IEEE Trans. Ind. Electron.*, vol. 56, no. 6, pp. 1894–1905, Jun. 2009, doi: 10.1109/TIE.2008.2007030.
[21] M. Preindl and S. Bolognani, "Model predictive direct speed control with finite control set of PMSM drive systems," *IEEE Trans. Power Electron.*, vol. 28, no. 2, pp. 1007–1015, Feb. 2013, doi: 10.1109/TPEL.2012.2204277.
[22] M. Siami, D. A. Khaburi, and J. Rodriguez, "Torque ripple reduction of predictive torque control for PMSM drives with parameter mismatch," *IEEE Trans. Power Electron.*, vol. 32, no. 9, pp. 7160–7168, Sep. 2017, doi: 10.1109/TPEL.2016.2630274.
[23] Y. Cho, W. J. Choi, and K.-B. Lee, "Model predictive control using a three-level inverter for induction motors with torque ripple reduction," in *Proc. ICIT Conf.*, Feb./Mar. 2014, pp. 187–192, doi: 10.1109/ICIT.2014.6894936.
[24] H. Zhu, X. Xiao, and Y. Li, "Torque ripple reduction of the torque predictive control scheme for permanent-magnet synchronous motors," *IEEE Trans. Ind. Electron.*, vol. 59, no. 2, pp. 871–877, Feb. 2012, doi: 10.1109/TIE.2011.2157278.
[25] Y. Cho, K.-B. Lee, J.-H. Song, and Y.-I. Lee, "Torque-ripple minimization and fast dynamic scheme for torque predictive control of permanent-magnet synchronous motors," *IEEE Trans. Power Electron.*, vol. 30, no. 4, pp. 2182–2190, Apr. 2015, doi: 10.1109/TPEL.2014.2326192.
[26] K.-K. Shyu, J.-K. Lin, V.-T. Pham, M.-J. Yang, and T.-W. Wang, "Global minimum torque ripple design for direct torque control of induction motor drives," *IEEE Trans. Ind. Electron.*, vol. 57, no. 9, pp. 3148–3156, Sep. 2010, doi: 10.1109/TIE.2009.2038401.
[27] Y. Zhang and J. Zhu, "A novel duty cycle control strategy to reduce both torque and flux ripples for DTC of permanent magnet synchronous motor drives with switching frequency reduction," *IEEE Trans. Power Electron.*, vol. 26, no. 10, pp. 3055–3067, Oct. 2011, doi: 10.1109/TPEL.2011.2129577.
[28] Y. Zhang and H. Yang, "Model predictive torque control of induction motor drives with optimal duty cycle control," *IEEE Trans. Power Electron.*, vol. 29, no. 12, pp. 6593–6603, Dec. 2014, doi: 10.1109/TPEL.2014.2302838.
[29] M. H. Vafaie, B. M. Dehkordi, P. Moallem, and A. Kiyoumarsi, "Minimizing torque and flux ripples and improving dynamic response of PMSM using a voltage vector with optimal parameters," *IEEE Trans. Ind. Electron.*, vol. 63, no. 6, pp. 3876–3888, Jun. 2016, doi: 10.1109/TIE.2015.2497251.

LETICIA ASEYE ADASE (Student Member, IEEE) received the B.S. degree in electrical and computer engineering from Ajou University, Suwon, South Korea, in 2018, where she is currently pursuing the M.S. degree. Her current research interests include electric machine drives and applications, power conversion, and reliability.

IBRAHIM MOHD ALSOFYANI (Member, IEEE) received the M.Eng. degree in electrical mechatronics and automatic control and the Ph.D. degree from Universiti Teknologi Malaysia, Johor Bahru, Malaysia, in 2011 and 2014, respectively. From 2014 to 2016, he was a Research Associate and then a Postdoctoral Fellow with the UTM-PROTON Future Drive Laboratory, Universiti Teknologi Malaysia. From 2016 to 2017, he was a Lecturer with the Faculty of Engineering, Lincoln University College, Selangor, Malaysia. In 2017, he joined the School of Electrical and Computer Engineering, Ajou University, Suwon, South Korea, as a Research Professor, where he became an Assistant Professor, in 2018. His current research interests include electric machine drives, renewable power generations, and electric vehicle applications. Dr. Alsofyani was a recipient of the Brain Korea 21 (BK21) Program Scholarship, in 2017.

KYO-BEUM LEE (Senior Member, IEEE) received the B.S. and M.S. degrees in electrical and electronic engineering from Ajou University, Suwon, South Korea, in 1997 and 1999, respectively, and the Ph.D. degree in electrical engineering from Korea University, Seoul, South Korea, in 2003. From 2003 to 2006, he was with the Institute of Energy Technology, Aalborg University, Aalborg, Denmark. From 2006 to 2007, he was with the Division of Electronics and Information Engineering, Chonbuk National University, Jeonju, South Korea. In 2007, he joined the Department of Electrical and Computer Engineering, Ajou University. His research interests include electric machine drives, renewable power generations, and electric vehicle applications. He is also an Associate Editor of the IEEE TRANSACTIONS ON POWER ELECTRONICS, the IEEE TRANSACTIONS ON INDUSTRIAL ELECTRONICS, the *Journal of Power Electronics*, and the *Journal of Electrical Engineering and Technology*.